

Collective dynamical skyrmion excitations in a magnonic crystal

M. Mruczkiewicz,^{1,2,3,*} P. Gruszecki,¹ M. Zelent,¹ and M. Krawczyk^{1,†}

¹*Faculty of Physics, Adam Mickiewicz University in Poznan, Umultowska 85, Poznań, PL-61-614 Poland*

²*Laboratoire Ondes et Matière d'Aquitaine, Université Bordeaux, CNRS, F-33405 Talence, France*

³*Institute of Electrical Engineering, Slovak Academy of Sciences, Dubravská Cesta 9, SK-841-04 Bratislava, Slovakia*

(Received 2 March 2015; revised manuscript received 11 May 2016; published 31 May 2016)

We investigate theoretically the magnetization dynamics in a skyrmion magnonic crystal. Collective excitations are studied in a chain of touching ferromagnetic nanodots in a skyrmion magnetic configuration. The determined dispersion relation of coupled skyrmions shows a periodic dependence on the wave vector, a characteristic feature of the band structure in magnonic crystals. By spatial analysis of the magnetization amplitude in the magnonic bands we identify the excited modes as breathing and clockwise gyrotropic dynamic skyrmions. Propagating with a negative and positive group velocity, respectively, these high- and low-frequency excitations can be further explored theoretically and experimentally for fundamental properties and technological applications in spintronics and magnonics.

DOI: [10.1103/PhysRevB.93.174429](https://doi.org/10.1103/PhysRevB.93.174429)

I. INTRODUCTION

Exotic spin textures can occur in ferromagnetic materials in low magnetic fields and temperatures as a result of the Dzyaloshinskii-Moriya interaction (DMI). Concurrent dipole-dipole interaction, exchange interaction, DMI, and anisotropy field can lead to the spontaneous realization of various magnetization arrangements, such as helical [1], conical [2] or skyrmion spin textures [3–8]. It has been shown that a single skyrmion can nucleate in an isolated ferromagnetic disk of nanometer size [9–12], or an array of skyrmions can emerge in an ultrathin film to form a skyrmion crystal (SkX) [13,14]. Skyrmions can be controlled by electric current, which is predicted to be several orders of magnitude lower than that required for controlling domain walls [11]. Therefore, since their discovery in magnetic textures, skyrmions have been considered for applications in memory devices [15], magnetic racetracks [16], and logic devices [17].

Dynamic excitations of skyrmions and SkXs have been investigated in terms of, e.g., interaction between a skyrmion and a magnetic droplet [18], and spin-wave (SW) scattering on a single skyrmion [19]. Resonant magnetization oscillations have been demonstrated to occur in a single skyrmion under the influence of an external dynamic magnetic field, with breathing [9,18–22], clockwise gyrotropic and counterclockwise gyrotropic modes identified [20–23]. Studies on the dynamics of coupled skyrmions [24] and their collective excitations [8,25] have demonstrated that it could be controlled with an external field.

In this paper we present a numerical study of the collective skyrmion dynamics in a chain of touching magnetic nanodots with skyrmion texture. The studied system is analogical to that considered in Ref. [26], where collective vortex excitations are investigated. However, in our study the dots are in the skyrmion state, their edges touch, and their diameter is almost two orders of magnitude smaller. We show that collective skyrmion dynamics can occur in such one-dimensional (1D)

magnonic crystals due to the coupling between nanodots. We also demonstrate that a dynamic signal can be transmitted through the chain in separate bands related to the breathing and gyrotropic modes, the basic excitations of a skyrmion in a single nanodot. These high- and low-frequency bands are characterized by positive and negative group velocities, respectively. We verify numerically that the existence of these collective skyrmion excitations in an array of nanodots is resistant to change in the diameter of the nanodots and the magnitude of the external magnetic field.

The paper is organized as follows. In Sec. II we present our model and describe the procedure of the performed micromagnetic simulations. In Sec. III we discuss the stability of a skyrmion in a single nanodisk and its basic excitation spectrum. The collective dynamics in a chain of nanodisks is considered in Sec. IV, in which we present and interpret the results of our numerical simulations. The study is summarized in the closing Sec. V.

II. MODEL

We investigate the skyrmion dynamics in a thin ($d = 1$ nm thick) circular ferromagnetic dot with a diameter D equal to 30 nm, 40 nm, 50 nm, 60 nm, 80 nm, and 100 nm; then we extend the system to a chain of equal dots with respective diameters. Composed of nonoverlapping dots arranged without gaps, the chain represents a 1D skyrmion magnonic crystal with a period a equal to the diameter of the dot.

We perform finite-difference time-domain (FDTD) simulations with a mumax³ solver [27], using a uniformly discretized grid with the size of the cell in the range $(0.5\text{--}1.0)\text{ nm} \times (0.5\text{--}1.0)\text{ nm} \times 1.0\text{ nm}$.

In the simulations we solve the Landau-Lifshitz equation in which the time derivative $\frac{\partial \mathbf{M}(\mathbf{r}, t)}{\partial t}$ is defined as the torque τ , and equal to

$$\tau = \gamma \frac{1}{1 + \alpha^2} (\mathbf{M} \times \mathbf{B}_{\text{eff}} + \alpha (\mathbf{M} \times (\mathbf{M} \times \mathbf{B}_{\text{eff}}))), \quad (1)$$

where α is a dimensionless damping parameter, and \mathbf{B}_{eff} is the effective magnetic induction field, which can include the external magnetic field \mathbf{B}_z , the magnetostatic demagnetizing

*m.mru@amu.edu.pl

†krawczyk@amu.edu.pl

field $\mathbf{B}_{\text{demag}}$, the Heisenberg exchange field \mathbf{B}_{exch} , the Dzyaloshinskii-Moriya exchange field \mathbf{B}_{DM} , and the magnetocrystalline anisotropy field \mathbf{B}_{anis} [27]:

$$\mathbf{B}_{\text{eff}} = \mathbf{B}_z + \mathbf{B}_{\text{demag}} + \mathbf{B}_{\text{exch}} + \mathbf{B}_{\text{DM}} + \mathbf{B}_{\text{anis}}. \quad (2)$$

The micromagnetic simulations take account of the influence of the DMI on the magnetization orientation at the nanodot edges, which results in magnetization bending there [27,28]. For more details on the numerical simulations please refer to the Appendix.

We use a set of parameters, which can be regarded as describing a sample multilayered thin film with a perpendicular magnetic anisotropy and DMI induced at the interfaces of the structure, where skyrmions can stabilize [5,9]. In such thin multilayered structures the magnetic anisotropy and the DMI can be considered homogeneous across the thickness of the multilayer and approximated to a constant [28,29]. The material parameter values assumed in our simulations correspond closely to those of a Pt/Co multilayer and have already been used in Refs. [5,9]. Ultrathin Pt/Co layers with a total thickness below 4 nm can be realized experimentally [30]. The parameter values used in the present study are magnetization saturation $M_S = 10^6$ A/m, exchange constant $A_{\text{ex}} = 1.5 \times 10^{-11}$ J/m, uniaxial anisotropy constant $K_{\text{ul}} = 10^6$ J/m³ (uniaxial anisotropy is perpendicular to the film plane), DMI constant $D_{\text{ind}} = 0.003$ J/m², and damping parameter $\alpha = 0.0001$. The assumed damping parameter value is reduced with respect to the literature value for better resolution of the dispersion relation in the simulations, to facilitate the interpretation of the numerical results. The external magnetic field B_z used in the calculations is kept out of plane, oriented along the z axis.

III. SKYRMION IN A DISK AND ITS DYNAMICS

The first structure to be considered is an isolated disk with a diameter $D = 30$ nm in a static magnetic field $B_z = 0.1$ T. The dynamics of skyrmions in an isolated disk has already been investigated and our simulations are in agreement with the reported results [9].

The ground state of the considered isolated disk is presented in Fig. 1(a). Upon excitation of the magnetization dynamics in the disk with a dynamic magnetic field (see Appendix) we observed two skyrmion modes below the cutoff frequency f_{signal} of the excitation signal, later identified as a clockwise gyrotropic mode m_{CW} excited with an in-plane external microwave magnetic field at $f_{\text{CW}} = 0.98$ GHz, and a breathing mode m_{Br} excited with an out-of-plane microwave magnetic field at $f_{\text{Br}} = 13.24$ GHz. An additional mode also exists in the investigated structure, however, at frequency 30.19 GHz, well above f_{signal} as was verified by the independent simulations. This mode exhibits the properties of the counterclockwise gyrotropic mode or azimuthal spin wave mode as discussed in [22,23,31].

We applied the discrete-time Fourier transform (DTFT) to each magnetization component at each point of the two-dimensional (2D) spatial grid, and plotted the DTFT values at the frequencies of interest versus x and y . The function obtained in this way represents the spatial distribution of the amplitude of the dynamic magnetization vector $\delta\mathbf{m}^j(x, y)$ [its

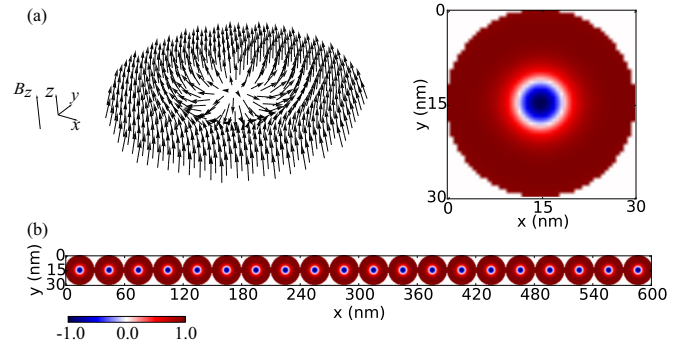


FIG. 1. Structures considered in this study, with an out-of-plane bias magnetic field B_z directed along the z axis. (a) Magnetic configuration in a single dot (left) and spatial distribution $m_z(x, y, t_0)$ of the z component of magnetization (right) at the starting time t_0 of the dynamic simulations. (b) Array of 20 nanodisks with a diameter of 30 nm: the $m_z(x, y, t_0)$ magnetization component plotted in the x, y plane.

real and imaginary parts, $\text{Re}(\delta\mathbf{m}^j)$ and $\text{Im}(\delta\mathbf{m}^j)$, respectively] of a mode j , and can be used for determining the change over time in the magnetization vector: $\Delta\mathbf{m}^j(x, y, t) = \mathbf{m}^j(x, y, t) - \mathbf{m}^j(x, y, t_0) = \text{Re}(\delta\mathbf{m}^j(x, y)e^{i2\pi f_j t})$.

Thus, the harmonic oscillations of the magnetization vector components at the frequency f_j of the j th mode are

$$m_i^j(x, y, t) = m_i^j(x, y, t_0) + \text{Re}(\delta m_i^j(x, y)e^{i2\pi f_j t}), \quad (3)$$

where the subscript i stands for x, y or z ; m_i is the corresponding Cartesian component of the magnetization vector normalized to 1, and $m_i(x, y, t_0)$ is the static equilibrium distribution of m_i in the x, y plane.

The amplitude and phase of the dynamic magnetization vector components in both eigenexcitations are shown in Fig. 2. Figure 3 presents four time snapshots of the magnetization in a single dot, taken at time intervals representing 1/4 of the oscillation period ($0.25 \times 1/f$). The low-frequency mode clearly shows gyrotropic oscillations, and can be identified as a clockwise gyrotropic mode m_{CW} [Figs. 2(a) and 3(a)]. This is indicated by the distribution of the δm_z magnetization component, with the largest amplitude distributed in a ring, along which the phase oscillates from $-\pi$ to π . Shown in Fig. 3(b), the high-frequency mode is a breathing mode m_{Br} . The amplitude of the z component of the magnetization vector in this mode forms a ring, is concentrated in the center of the disk, and has a constant phase sign there; this means that the skyrmion is dynamically expanding and compressing [see Fig. 2(b)]. The images shown in Fig. 2 will help us establish the character of collective excitations in an array of disks considered in the next section.

IV. COLLECTIVE EXCITATIONS

By extending the system to a chain of closely packed nanodisks we create a 1D skyrmion magnonic crystal. Figure 1(b) shows the distribution of $m_z(x, y, t_0)$ in an array of 20 1-nm-thick nanodisks with a diameter of 30 nm. In order to obtain the dispersion relation of dynamic skyrmions we use the 2D Fourier transform (2DFT) from the space-and-time domain

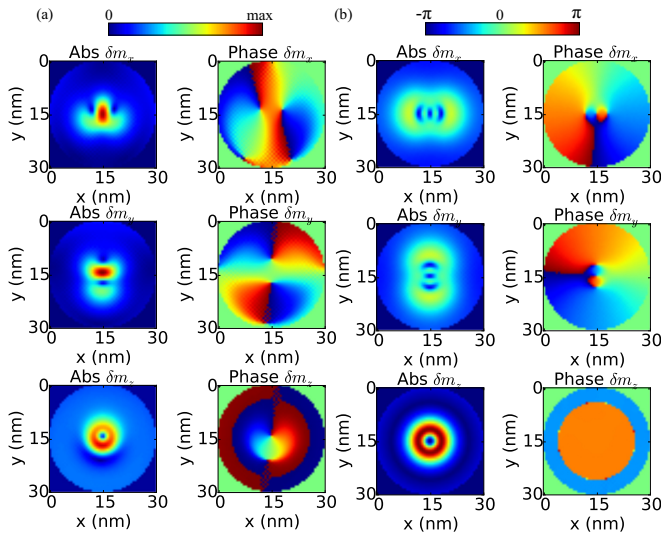


FIG. 2. Spatial maps of the x , y , and z components of the dynamic magnetization vector $\delta\mathbf{m}$ of (a) the 0.98 GHz clockwise gyrotropic mode, and (b) the 13.24 GHz breathing mode, obtained from FDTD simulations in a 30-nm nanodot under magnetic field $B_z = 0.1$ T. Left and right columns show the absolute value and phase, respectively, of each $\delta\mathbf{m}$ component.

(x, t) to the wave number-and-frequency domain (k, f) ; the 2DFT is applied to the magnetization component $m_z(x, y, t)$ along the z axis at the value of y corresponding to the center of the dots.

Figure 4 shows the calculated dispersion relation of dynamic skyrmions in this chain, with an out-of-plane excitation magnetic field b_{dyn} applied locally to the central disk No. 9 (see

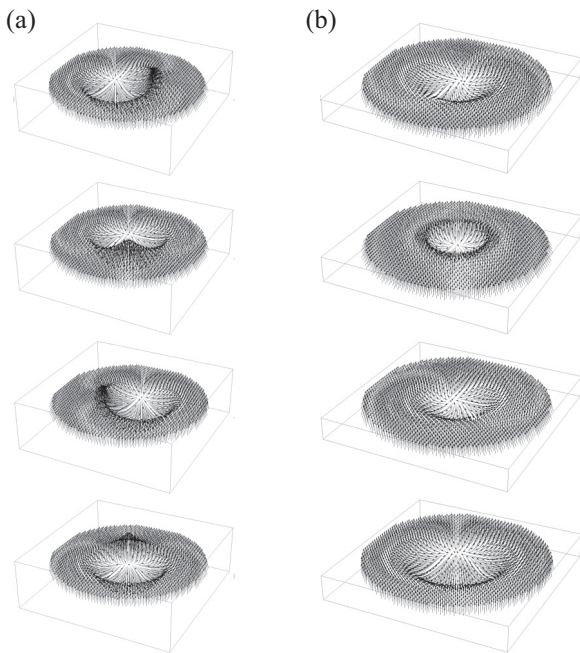


FIG. 3. Time snapshots of the dynamic skyrmion excitations, taken at intervals representing 1/4 of the oscillation period: (a) clockwise gyrotropic mode; (b) breathing mode.

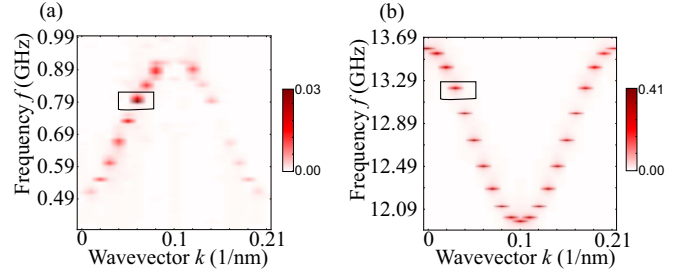


FIG. 4. Function $|2\text{DFT}|$ showing the dispersion relation of collective (a) clockwise gyrotropic and (b) breathing skyrmion excitations. In each graph $|2\text{DFT}|$ is normalized to the maximum value. The signal magnitude in (a) is approximately 10 times weaker than in (b). Black squares indicate results corresponding to wave numbers considered further in this paper.

Appendix for details). Two magnonic bands are found below the cutoff frequency f_{signal} of the excitation signal. Both have a clearly periodic wave number dependence, with a period equal to the magnitude of the reciprocal lattice vector $\frac{2\pi}{a}$, and a Brillouin zone (BZ) boundary at $k = \pi/a \approx 0.1 \text{ nm}^{-1}$, where a is the lattice constant.

These two frequency bands span from 0.49 to 0.99 GHz and from 11.88 to 13.68 GHz, which corresponds to the frequencies of the modes found in the isolated dot. This suggests that the observed bands are related to clockwise gyrotropic and breathing modes, respectively. In order to verify the character of excitations in these bands we visualize the spatial distribution of the dynamic magnetization component δm_z for selected wave numbers, marked with black squares in Fig. 4, according to the procedure described in Ref. [32] and in the Appendix. The results are presented in Figs. 5(a)–5(d). The spatial distributions of the absolute value and phase of the z component of the magnetization vector in the magnonic crystal

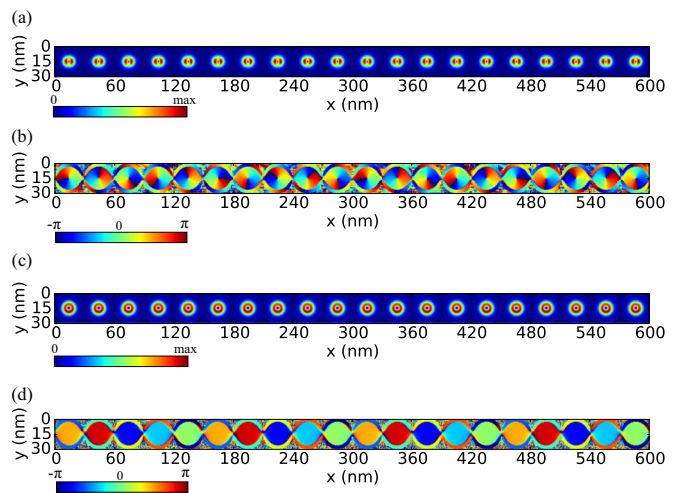


FIG. 5. Collective skyrmion spin-wave excitations in a chain of 30-nm nanodisks in a 0.1-T out-of-plane external magnetic field. (a) Absolute value of δm_z and (b) its phase in the collective clockwise gyrotropic mode with wave number $k = 0.6 \frac{\pi}{a}$. (c) Absolute value of δm_z and (d) its phase in the collective breathing mode with wave number $k = 0.4 \frac{\pi}{a}$.

are comparable with the respective spatial distributions in the isolated disk, shown in Figs. 2(a) and 2(b). This confirms the gyrotropic and breathing character of collective excitations in the lower and higher band, respectively. The phase distribution in Fig. 5 shows a shift in neighboring disks, which corresponds to the wavelength of the analyzed mode.

We also performed the simulations with a realistic value $\alpha = 0.01$ of the intrinsic magnetic damping constant in Co [33]. The calculated group velocities of the breathing and gyrotropic modes at $k \approx \pi/4a$ are -96 m/s and 30 m/s, respectively. The estimated lifetime of the breathing mode is around 1.2 ns (at $f = 12.984$ GHz), which corresponds to a propagation length of 113 nm. The low value of the propagation length is due to the low group velocities of skyrmion modes in the studied system. Better performance would require materials with lower damping, or a structure design providing higher group velocities.

In the investigated system the breathing mode band is more than three times wider than the clockwise gyrotropic mode band, which indicates stronger coupling between breathing oscillations in the disks. Moreover, as we have observed in Fig. 4, the group velocities in the two bands have opposite signs. These two features suggest that different coupling mechanisms are responsible for propagation in each band. Below we will explain qualitatively a possible origin of these two types of dynamic interaction in a skyrmion chain.

As we have established in Sec. III, the breathing mode has dominating oscillations of the m_z magnetization component, but weak and antisymmetric oscillations of the m_x and m_y components [see Fig. 2(b)]. This suggests that the coupling between breathing excitations in nanodots in the chain can be realized via a microwave demagnetizing field $\delta B_{\text{demag},z}(t)$ generated by the out-of-plane component of the magnetization vector above (or below) the disks (see Fig. 6). This demagnetizing field oscillates in phase with $\delta m_z(t)$ above (and below) the disk and in antiphase beyond the disk area in the disk plane.

Let us consider two neighboring skyrmions at sites i and $i + 1$, and estimate the energy E of dynamic interaction at site $i + 1$ due to the demagnetizing field generated by the i th skyrmion when their breathing modes are in phase or in antiphase. The dynamic interaction energy obeys the proportionality:

$$E \propto -\delta m_{z,i+1}(t) \cdot \delta B_{\text{demag},z,i}(t). \quad (4)$$

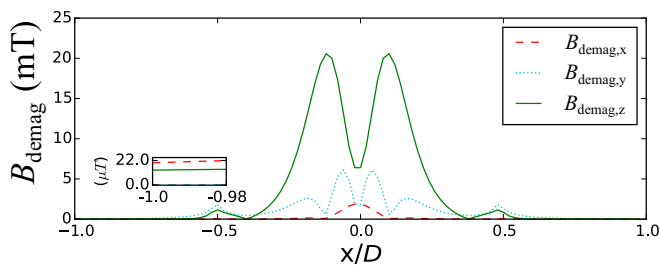


FIG. 6. Absolute values of the amplitude of the x , y , and z components of the dynamic demagnetizing field $\delta \mathbf{B}_{\text{demag}}$ in the breathing mode (13.86 GHz) in a 30-nm dot in a 0.05-T external magnetic field. Plotted along the x axis, the amplitude profiles follow the line passing through the center of the isolated dot.

When $\delta m_{z,i}$ and $\delta m_{z,i+1}$ oscillate in phase, the dynamic demagnetizing field $\delta B_{\text{demag},z,i}(t)$ induced by the i th skyrmion at site $i + 1$ will oscillate in antiphase with $\delta m_{z,i}$. The interaction energy E will be proportional to $|\delta m_{z,i+1} \cdot \delta B_{\text{demag},z,i}|$. In the case of antiphase oscillations of the skyrmion modes the energy of interaction will be proportional to $-|\delta m_{z,i+1} \cdot \delta B_{\text{demag},z,i}|$. Thus, antiphase or in-phase oscillations of neighboring skyrmions will decrease or increase, respectively, the interaction energy, and consequently, the frequency of collective excitations.

In magnonic crystals antiphase oscillations occur at the boundary of the BZ, where the excitation wavelength is equal to $2a$, while in the BZ center all the nanodots oscillate in phase, against the dipolar coupling defined in Eq. (4). This qualitatively explains the decrease in the frequency of the breathing mode with increasing wave number in the first BZ, i.e., the negative group velocity, shown in Fig. 4(b). Additionally, since the disks in the array are in direct contact, also the exchange interaction can contribute to the dispersion relation. However, we have verified and confirmed numerically that the group velocity of the breathing mode will remain negative also in a chain of separate disks.

In the gyrotropic mode the interaction is governed by the effective net magnetization induced by the core shift. These oscillations are similar to the gyrotropic modes in nanodots in the vortex state, in which positive group velocity was observed as well [26,34–38].

Whereas in the isolated disk under the out-of-plane microwave magnetic field we only observe a breathing mode; in the array of dots two branches are excited with an out-of-plane dynamic magnetic field. This is most probably due to static magnetodipolar interaction between neighboring disks, which alters the symmetry of the eigenstate of the isolated disk. More specifically, the symmetry of the z component is broken, resulting in a nonzero overlapping integral under the out-of-plane external magnetic field. This hypothesis is confirmed by the data presented in Figs. 2 and 6, showing the distribution of the amplitude of dynamic magnetization and the magnitude of the dynamic demagnetizing field, respectively.

In the gyrotropic mode the overlapping integral between the z component of the dynamic demagnetizing field and δm_z is close to zero, since there is antisymmetry between the δm_z distribution and the in-phase oscillations of the demagnetizing field in the area of possible interaction. Thus, the interaction between gyrotropic excitations is governed by the x and y components of the dynamic dipolar field. In this case the weak coupling results in a narrow band of gyrotropic excitations, with a bandwidth around 0.5 GHz, against 1.6 GHz for the breathing mode (see Fig. 4).

Now, let us investigate the influence of the nanodot size and the external magnetic field magnitude on the skyrmions and their collective excitations. Figure 7(a) shows the distribution of the ground-state magnetization $m_z(x, y, t_0)$ and the static components of the demagnetizing and effective magnetic fields in 1-nm-thick disks of different size, with a diameter of 30, 40, 50, and 100 nm, in magnetic field $B_z = 0.1$ T; the profiles are plotted along the line in the x direction passing through the center of the disk. The position on the horizontal axis is normalized to the diameter of the disk. In all the dots the skyrmions are stable, but vary widely in

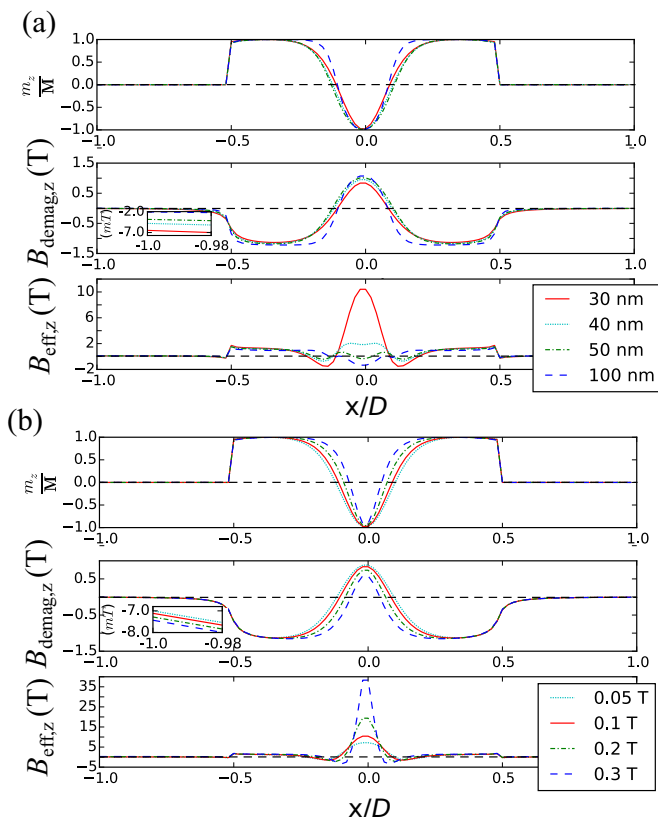


FIG. 7. Influence of the (a) disk diameter (D) and (b) magnetic field magnitude (B_z) variation on the ground-state magnetization distribution (m_z), z components of the static demagnetizing ($B_{\text{demag},z}$), and z components of effective magnetic fields ($B_{\text{eff},z}$) in the dot. On the horizontal axis, the position along the center of the dot is in reduced units.

size. However, when normalized, the size of the skyrmions, delimited by $m_z = 0$, remains almost constant. Changing the size of the disk affects also the demagnetizing field in and beyond the disk [see the middle panel in Fig. 7(a)]. The magnitude of the demagnetizing field outside of the disk decreases significantly with increasing disk size (see the inset), which indicates decreasing coupling between neighboring disks. However, it is the effective magnetic field that proves the most sensitive to the disk size. Since the size of the skyrmion decreases with decreasing size of the disk, the magnetization gradient increases accordingly, resulting in high values of the exchange field, which becomes the dominating component of the effective field.

Figure 8(a) presents the dispersion relation of the collective breathing excitation in a chain of disks with a diameter of 50 nm with skyrmion texture. As compared to the case of 30-nm disks (Fig. 4), the band is much narrower and shifted to lower frequencies. The decrease in the frequency is connected with the lower frequency of the breathing mode in the larger isolated dot; the reduced bandwidth indicates weaker dynamic coupling, due to a decrease in the demagnetizing field beyond the disk with increasing size of the dot.

In Fig. 9 we present cumulative data on the influence of the disk diameter (skyrmion size scales proportionally)

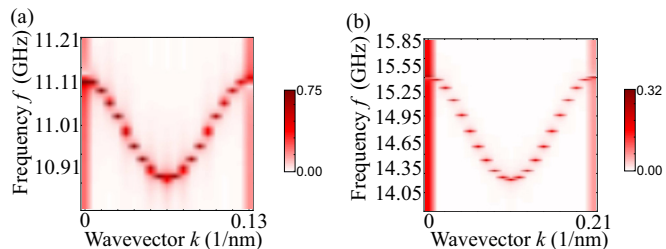


FIG. 8. Dispersion relation of the breathing excitation in an array of (a) 50-nm disks under external magnetic field $B_z = 0.1$ T; (b) 30-nm disks under external magnetic field $B_z = 0.2$ T.

on the bandwidth Δf of the CW gyrotropic (blue squares) and breathing (black circles) modes. The decrease in both bandwidths with increasing dot size indicates a decrease in the disk coupling. In small disks the breathing band is more than three times wider than the gyrotropic band, but the difference decreases with increasing dot diameter. In larger disks, with a diameter above 50 nm, the collective gyrotropic modes are not effectively excited by an out-of-plane field.

We have also studied an isolated disk with a diameter of 30 nm under external magnetic field of different magnitudes: 0.05, 0.1, 0.2, and 0.3 T. Figure 7(b) shows the calculated static distributions of the z component of the magnetization, and the distributions of the z components of the magnetic fields B_{demag} and B_{eff} . The magnitude of the external magnetic field is found to affect the size of the skyrmion [9]. In a magnetic field opposite the polarization of the skyrmion center the skyrmion will shrink with increasing B_z [top panel in Fig. 7(b)]. Consequently, the exchange field in the skyrmion will increase, resulting in a significant increase in the effective field in the center of the dot, as shown in the bottom panel of Fig. 7(b). The observed decrease in the size of the skyrmion with increasing magnetic field will shift the breathing mode to higher frequencies. However, in a dot chain the coupling between breathing excitations can decrease due to the increase in the separation between skyrmions with their decreasing size.

The dispersion relation in an array of 30-nm disks under a 0.2-T external magnetic field is presented in Fig. 8(b). As

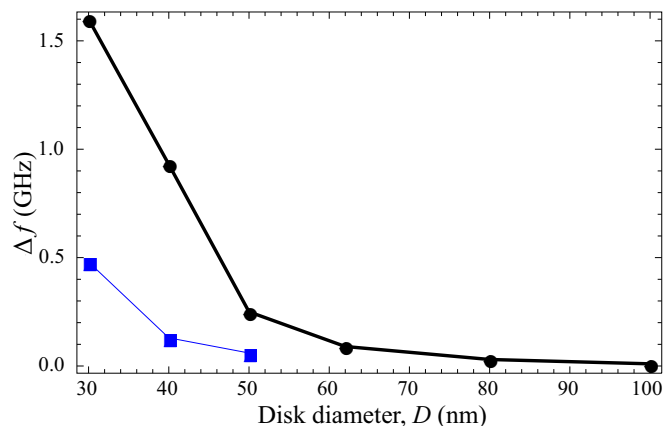


FIG. 9. Bandwidth Δf of the CW gyrotropic (blue squares) and breathing (black circles) modes in an array of dots versus dot diameter D .

expected, the band is shifted to higher frequencies with respect to that observed in a 0.1-T field [Fig. 4(b)], and its width is reduced from 1.6 to 1.2 GHz.

V. SUMMARY

We have shown that a magnonic band structure based on skyrmion excitations is possible in an array of nanodisks with DMI. Using micromagnetic simulations, we have demonstrated the dispersive character and collective properties of two types of excitations observed in the considered system: gyrotropic and breathing skyrmion modes, characterized by positive and negative group velocities, respectively. The bandwidth of the breathing oscillations is approximately three times larger than the width of the gyrotropic band, indicating a significant coupling between breathing skyrmion oscillations in touching nanodots. We have also analyzed the influence of the dot size and the magnitude of the external magnetic field on the observed skyrmions and their coupling. We have found an increase in the effective magnetic field generated by skyrmions in small dots under low magnetic fields opposite the skyrmion center.

The results presented in this paper can be verified experimentally by time-resolved scanning transmission x-ray microscopy (STXM) [26]. The predicted spin-wave signal propagation in a skyrmion chain can be also measured by all-electrical spin-wave spectroscopy [8].

Analogically to collective vortex excitations, the skyrmion dynamics could be used for the realization of logic devices [37,39] operating at high frequencies and using a fraction of the energy consumed by electronic logic gates. Another interesting potential application of 1D magnonic crystals with collective skyrmion excitations is related to their combination with the recently demonstrated single-dot excitation of skyrmions by spin torque nano-oscillators [40].

ACKNOWLEDGMENTS

The project is financed by the SASPRO Programme. The research leading to these results has received funding from the People Programme (Marie Curie Actions) European Union's Seventh Framework Programme under REA Grant Agreement No. 609427 (Project WEST, 1244/02/01). Research has been further co-funded by the Slovak Academy of Sciences, Polish National Science Centre Project No. DEC-2012/07/E/ST3/00538, and the European Union Horizon 2020 Research and Innovation Programme under Marie Skłodowska-Curie Grant Agreement No. 644348 (MagIC).

The numerical calculations were performed at Poznan Supercomputing and Networking Center (Grant No. 209). P.G. acknowledges support from the Adam Mickiewicz University Foundation.

APPENDIX: MICROMAGNETIC SIMULATIONS

The micromagnetic simulations were performed in two stages. In the first stage the initial magnetization configuration was postulated with a Néel skyrmion in the center of each dot. The system was relaxed to achieve the energy minimum (we have used the `relax()` function in `mumax3`). Stabilized magnetization vector distributions $m_x(x, y, t_0)$, $m_y(x, y, t_0)$, and $m_z(x, y, t_0)$ were obtained by this procedure.

In the second stage we performed the simulations of magnetization dynamics. The magnetization distribution obtained in the first stage was put under an alternating external magnetic field b_{dyn} directed either out of plane (along the z axis) or in plane (along the x axis). The dynamic field had a cutoff frequency $f_{\text{signal}} = 16$ GHz and was shifted in time by $t_{\text{shift}} = 10^{-9}$ s: $b_{\text{dyn}} = b_{\text{amp}} \text{sinc}[2\pi f_{\text{signal}}(t - t_{\text{shift}})]$. The amplitude parameter b_{amp} of the sinc signal was chosen so that the maximum absolute value of the dynamic magnetic field was 0.01 T. The excitation field b_{dyn} was uniform and limited to the dot.

In the dynamic simulations we use the Dormand-Prince method with an adaptive time step control for advancing the Landau-Lifshitz equation. The maximum time step was set to 10^{-12} s and the minimum time step to 10^{-15} s. The total time of the simulations was limited to 3×10^{-7} s. The dynamic magnetization components were saved with a sampling interval of 3×10^{-11} s. Such specification allows one to perform the Fourier transform to the frequency domain with a resolution below 10 MHz within the range $(0, f_{\text{signal}})$.

In order to determine the character of the modes we visualized the spatial distribution of the dynamic magnetization component δm_z following the procedure described in Ref. [32]. We applied the 2DFT to m_z for each value of y . In the next step, for each frequency we defined a 1D vector to which we assigned the corresponding value of the 2DFT. We chose a wave number k and kept the 2DFT values for all the wave numbers differing from k by a multiple of the reciprocal lattice vector $\mathbf{G} = 2\pi/a$, i.e., for $k \pm nG$, where n is an integer and a the lattice constant (30 nm or 50 nm in our simulations). For the other wave numbers the value was set to zero. Finally, we performed the inverse Fourier transformation to obtain the dynamic magnetization component δm_z for each mode with a specific frequency and wave number.

-
- [1] H. Kwon and C. Won, *J. Magn. Magn. Mater.* **351**, 8 (2014).
 - [2] I. V. Bychkov, D. A. Kuzmin, and V. G. Shavrov, *J. Magn. Magn. Mater.* **329**, 142 (2013).
 - [3] T. H. R. Skyrme, *Nuclear Physics* **31**, 556 (1962).
 - [4] F. Ma and Y. Zhou, *RSC Adv.* **4**, 46454 (2014).
 - [5] F. Garcia-Sanchez, P. Borys, A. Vansteenkiste, J. V. Kim, and R. L. Stamps, *Phys. Rev. B* **89**, 224408 (2014).
 - [6] X. Zhang, T. Liu, M. E. Flatté, and H. X. Tang, *Phys. Rev. Lett.* **113**, 037202 (2014).
 - [7] M. Y. Im, P. Fischer, K. Yamada, T. Sato, S. Kasai, Y. Nakatani, and T. Ono, *Nature Communications* **3**, 983 (2012).
 - [8] T. Schwarze, J. Wäizner, M. Garst, A. Bauer, I. Stasinopoulos, H. Berger, C. Pfeleiderer, and D. Grundler, *Nat. Mater.* **14**, 478 (2015).
 - [9] J. V. Kim, F. Garcia-Sanchez, J. Sampaio, C. Moreau-Luchaire, V. Cros, and A. Fert, *Phys. Rev. B* **90**, 064410 (2014).
 - [10] H. Du, W. Ning, M. Tian, and Y. Zhang, *Phys. Rev. B* **87**, 014401 (2013).

- [11] J. Sampaio, V. Cros, S. Rohart, A. Thiaville, and A. Fert, *Nat. Nanotechnol.* **8**, 839 (2013).
- [12] K. Guslienko, *Magnetics Letters, IEEE* **6**, 1 (2015).
- [13] H. Kwon, K. Bu, Y. Wu, and C. Won, *J. Magn. Magn. Mater.* **324**, 2171 (2012).
- [14] M. N. Wilson, A. B. Butenko, A. N. Bogdanov, and T. L. Monchesky, *Phys. Rev. B* **89**, 094411 (2014).
- [15] N. Kiselev, A. Bogdanov, R. Schäfer, and U. Röbber, *J. Phys. D* **44**, 392001 (2011).
- [16] R. Tomasello, E. Martinez, R. Zivieri, L. Torres, M. Carpentieri, and G. Finocchio, *Sci. Rep.* **4**, 6784 (2014).
- [17] X. Zhang, M. Ezawa, and Y. Zhou, *Sci. Rep.* **5**, 11369 (2015).
- [18] Y. Zhou, E. Iacocca, A. A. Awad, R. K. Dumas, F. C. Zhang, H. B. Braun, and J. Åkerman, *Nat. Commun.* **6**, 8193 (2015).
- [19] C. Schütte and M. Garst, *Phys. Rev. B* **90**, 094423 (2014).
- [20] Y. Dai, H. Wang, T. Yang, W. Ren, and Z. Zhang, *Sci. Rep.* **4**, 6153 (2014).
- [21] Y. Okamura, F. Kagawa, M. Mochizuki, M. Kubota, S. Seki, S. Ishiwata, M. Kawasaki, Y. Onose, and Y. Tokura, *Nat. Commun.* **4**, 2391 (2013).
- [22] Z. V. Gareeva and K. Y. Guslienko, *Phys. status solidi (RRL)-Rapid Res. Lett.* **10**, 227 (2016).
- [23] M. Mochizuki, *Phys. Rev. Lett.* **108**, 017601 (2012).
- [24] H. Wang, Y. Dai, T. Yang, W. Ren, and Z. Zhang, *RSC Advances* **4**, 62179 (2014).
- [25] J. Zang, M. Mostovoy, J. H. Han, and N. Nagaosa, *Phys. Rev. Lett.* **107**, 136804 (2011).
- [26] D. S. Han, A. Vogel, H. Jung, K. S. Lee, M. Weigand, H. Stoll, G. Schütz, P. Fischer, G. Meier, and S.-K. Kim, *Sci. Rep.* **3**, 2262 (2013).
- [27] A. Vansteenkiste, J. Leliaert, M. Dvornik, M. Helsen, F. Garcia-Sanchez, and B. Van Waeyenberge, *AIP Advances* **4**, 107133 (2014).
- [28] S. Rohart and A. Thiaville, *Phys. Rev. B* **88**, 184422 (2013).
- [29] A. Thiaville, S. Rohart, É. Jué, V. Cros, and A. Fert, *Europhys. Lett.* **100**, 57002 (2012).
- [30] I. M. Miron, T. Moore, H. Szabolcs, L. D. Buda-Prejbeanu, S. Auffret, B. Rodmacq, S. Pizzini, J. Vogel, M. Bonfim, A. Schuhl *et al.*, *Nat. Mater.* **10**, 419 (2011).
- [31] K. Y. Guslienko and Z. V. Gareeva, [arXiv:1603.0072](https://arxiv.org/abs/1603.0072).
- [32] D. Kumar, P. Sabareesan, W. Wang, H. Fangohr, and A. Barman, *J. Appl. Phys.* **114**, 023910 (2013).
- [33] A. Berger, W. Amamou, S. White, R. Adur, Y. Pu, R. Kawakami, and P. C. Hammel, *J. Appl. Phys.* **115**, 17C510 (2014).
- [34] A. Vogel, A. Drews, T. Kamionka, M. Bolte, and G. Meier, *Phys. Rev. Lett.* **105**, 037201 (2010).
- [35] S. Barman, A. Barman, and Y. Otani, *IEEE Trans. Magn.* **46**, 1342 (2010).
- [36] D.-S. Han, H.-B. Jeong, and S.-K. Kim, *Appl. Phys. Lett.* **103**, 112406 (2013).
- [37] D. Kumar, S. Barman, and A. Barman, *Sci. Rep.* **4**, 4108 (2014).
- [38] M. Asmat-Uceda, X. Cheng, X. Wang, D. J. Clarke, O. Tchernyshyov, and K. S. Buchanan, *J. Appl. Phys.* **117**, 123916 (2015).
- [39] H. Jung, Y. S. Choi, K. S. Lee, D. S. Han, Y. S. Yu, M. Y. Im, P. Fischer, and S. K. Kim, *ACS Nano* **6**, 3712 (2012).
- [40] S. Zhang, J. Wang, Q. Zheng, Q. Zhu, X. Liu, S. Chen, C. Jin, Q. Liu, C. Jia, and D. Xue, *New J. Phys.* **17**, 023061 (2015).